Journal of Molecular Spectroscopy **197,** 133–146 (1999)
Article ID jmsp.1999.7911, available online at http://www.idealibrary.com on IDEAL®

Emission Spectroscopy and *Ab Initio* Calculations on IrN

R. S. Ram,* J. Liévin,† and P. F. Bernath*,‡

*Department of Chemistry, University of Arizona, Tucson, Arizona 85721; †Université Libre de Bruxelles, Laboratoire de Chimie Physique Moléculaire, CP 160/09, Av. F. D. Roosevelt 50, Brussels, Belgium; and ‡Department of Chemistry, University of Waterloo, Waterloo, Ontario, Canada N2L 3G1

Received November 9, 1998; in revised form June 10, 1999

The emission spectrum of IrN was recorded in the near infrared using a Fourier transform spectrometer. The IrN molecules were excited in an Ir hollow cathode lamp operated with a mixture of Ne and a trace of N_2. Numerous IrN bands observed in the 7500–9200 cm^{-1} region were assigned to a new $a^3\Pi$–$X^1\Sigma^+$ electronic transition with the 0–0 bands of the $a^3\Pi_0$–$X^1\Sigma^+$ and $a^3\Pi_1$–$X^1\Sigma^+$ subbands near 9175 and 8841 cm^{-1}, respectively. A rotational analysis of several bands of the 0–0 and 0–1 sequences was obtained and molecular constants were extracted. The effective Hund's case (a) constants for the new $a^3\Pi$ state are: T_{00} = 8840.31747(88) cm^{-1}, A_0 = −340.53329(93) cm^{-1}, $\Delta G(1/2)$ = 984.3629(23) cm^{-1}, B_e = 0.4699116(27) cm^{-1}, α_e = 0.0030058(50) cm^{-1}, and r_e = 1.6576432(47) Å. The spectroscopic properties of the ground state and several low-lying electronic states of IrN were also predicted by ab initio calculations. These calculations are consistent with our assignment of the $a^3\Pi$–$X^1\Sigma^+$ transition and also support our previous assignments of the $A'\ ^1\Pi$ and $A^1\Pi$ electronic states [R. S. Ram and P. F. Bernath, *J. Mol. Spectrosc.* **193**, 363 (1999)]. The excited $a^3\Pi$ state of IrN has an $1\sigma^2 2\sigma^2 1\pi^4 3\sigma^1 1\delta^4 2\pi^1$ electron configuration and the configurations of the other low-lying electronic states are also discussed.

INTRODUCTION

The interaction of transition metals with nitrogen has important applications in catalysis and in surface science as well as for comparison with *ab initio* calculations. Diatomic transition metal nitrides also serve as simple models for the study of metal–nitrogen bonding in inorganic chemistry. Like several diatomic transition metal oxides (*1–4*) and hydrides (*5–8*), transition metal nitrides are also of potential astrophysical importance. For the 5*d* transition metal nitride family, high-resolution data are available for HfN (*9*), WN (*10*), ReN (*11*, *12*), OsN (*13*), IrN (*14*, *15*), and PtN (*16*, *17*). In spite of this experimental interest, no theoretical calculations are available for the 5*d* transition metal nitrides, except for PtN (*18*).

The first spectroscopic observation of IrN was made in 1996 by Marr *et al.* (*14*) who observed a $^1\Pi$–$^1\Sigma^+$ transition near 15 190 cm^{-1} by laser excitation spectroscopy. This transition was labeled as the $A^1\Pi$–$X^1\Sigma^+$ electronic transition by comparison with the isoelectronic PtC molecule (*19–22*). For PtC two additional low-lying electronic states labeled as $A'\ ^1\Pi$ and $A''\ ^1\Sigma^+$ were observed below the $A^1\Pi$ state (*21*). To locate the analogous $A'\ ^1\Pi$ and $A''\ ^1\Sigma^+$ states of IrN, we have recently investigated the spectrum of IrN in the 10 000–20 000 cm^{-1} region (*15*). In this work we identified a new $A'\ ^1\Pi$–$X^1\Sigma^+$ transition of IrN near 13 135 cm^{-1} and have observed numerous additional bands with vibrational levels up to v', v'' = 4 for the $A^1\Pi$–$X^1\Sigma^+$ transition. We have also noted interactions between the v = 0 and 1 vibrational levels of $A'\ ^1\Pi$ state and the v = 2 and 3 vibrational levels of $A^1\Pi$ state, causing global perturbations.

A comparison of the observed states of IrN and PtC indicated that an electronic state analogous to the $A''\ ^1\Sigma^+$ state of PtC remained to be observed for IrN. To search for this state we have recently recorded the spectrum of IrN below 10 000 cm^{-1}. Our spectra revealed the presence of two new transitions in the near infrared, one of the $^1\Sigma^+$–$X^1\Sigma^+$ type (ν_0 = 9181.8072 cm^{-1}) and the other of the $^1\Pi$–$X^1\Sigma^+$ type (ν_0 = 8841.2561 cm^{-1}). The $^1\Sigma^+$–$X^1\Sigma^+$ transition near 9182 cm^{-1} is most probably analogous to the $A''\ ^1\Sigma^+$–$X^1\Sigma^+$ transition of PtC. The observation of a nearby $^1\Pi$–$X^1\Sigma^+$ transition suggests that the two new transitions are the subbands of a $^3\Pi$–$X^1\Sigma^+$ transition. We have, therefore, assigned the two new infrared transitions as the $^3\Pi_0$–$^1\Sigma^+$ and $^3\Pi_1$–$^1\Sigma^+$ subbands of the $a^3\Pi$–$X^1\Sigma^+$ transition of IrN. The analysis of this transition is reported in this paper.

To better understand the electronic structure of IrN and to confirm the assignments, *ab initio* calculations were performed and the spectroscopic properties of several singlet and triplet states were calculated. Our assignments of the $X^1\Sigma^+$, $a^3\Pi$, $A'\ ^1\Pi$ and $A^1\Pi$ states and their observed spectroscopic parameters are in excellent agreement with the predictions of the *ab initio* calculations.

MATERIALS AND METHODS

The experimental conditions for the observation of the near infrared bands of IrN were the same as described in our previous paper (*15*). In summary, the IrN bands were produced in a hollow-cathode lamp by discharging a mixture of 2.5 Torr

0022-2852/99 $30.00

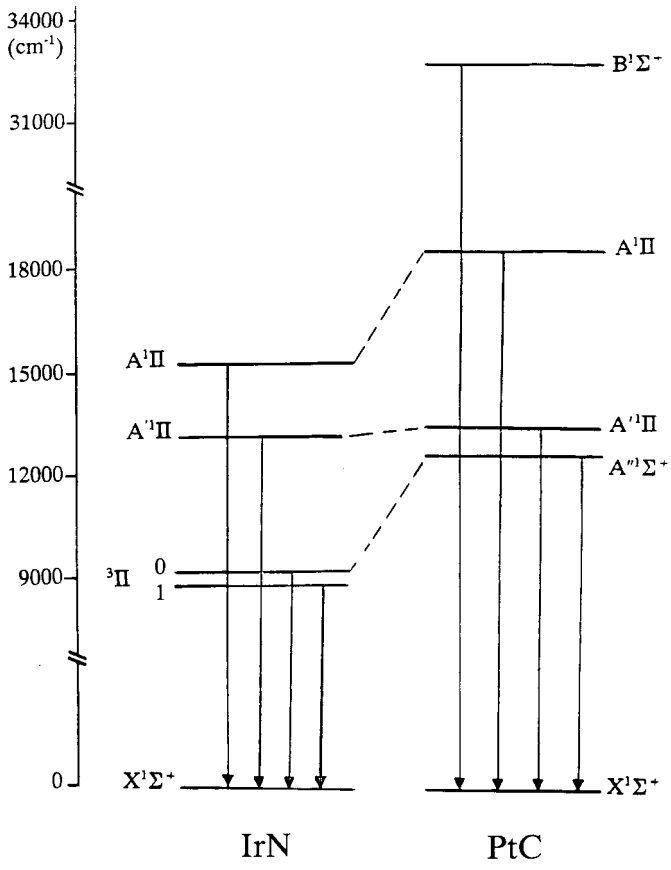

FIG. 1. A schematic energy level diagram of the known electronic states of IrN and PtC.

of Ne and about 10 mTorr of N_2 with 600 V and 310 mA current.

The spectra in the 3000–13 000 cm^{-1} region were recorded with the 1-m Fourier transform spectrometer associated with the McMath–Pierce solar telescope of the National Solar Observatory at Kitt Peak. The spectrometer was equipped with a CaF_2 beam splitter, InSb detectors, and red pass (Schott 780) filters. In total 30 scans were co-added in about 3.8 h of integration. In addition to the IrN bands, the observed spectra also contained Ir and Ne atomic lines as well as strong N_2 molecular lines. Although there is some overlapping from the N_2 bands, particularly in the 7000–8900 cm^{-1} region, the IrN bands were clearly distinguished by their smaller line spacing. We have calibrated our IrN spectra using the measurements of Ne atomic lines made by Palmer and Engleman (*23*). The spectra were measured using a program called PC-DECOMP developed by J. Brault. The peak positions were determined by fitting a Voigt lineshape function to each spectral feature. The absolute accuracy of the wavenumber scale is expected to be on the order of ± 0.002 cm^{-1}. The strong lines of IrN appear with a typical signal-to-noise ratio of 10:1 and the precision of measurements of strong and unblended IrN lines is expected to be better than ± 0.003 cm^{-1}.

AB INITIO CALCULATIONS

Ab initio calculations were performed on the low-lying Σ^+, Π, Δ, and Φ states of singlet and triplet spin multiplicities of IrN. The same computational approach as in our recent work on RuN (*24*) was adopted. It consists of a complete active space self-consistent field (CASSCF) calculation (*25*) followed by an internally contracted multireference configuration interaction (CMRCI) (*26*) calculation. All valence orbitals, i.e., the four σ, two π, and one δ orbitals arising from the 5*d* and 6*s* orbitals of iridium and the 2*s* and 2*p* orbitals of nitrogen, were optimized at the CASSCF level. A state averaging procedure was used to optimize a common molecular orbital basis set for describing the states of interest in a given spin multiplicity. These orbitals were then used in a second step for a CMRCI calculation in which all valence electrons were correlated. The CMRCI energies were corrected for Davidson's contribution (*27*) for unlinked four-particle clusters. The quasi-relativistic peudo-potentials and the corresponding basis sets, developed in Stuttgart, were used to represent the 60 core electrons of the iridium atom (*28*). This core does not include the 5*s* and 5*p*

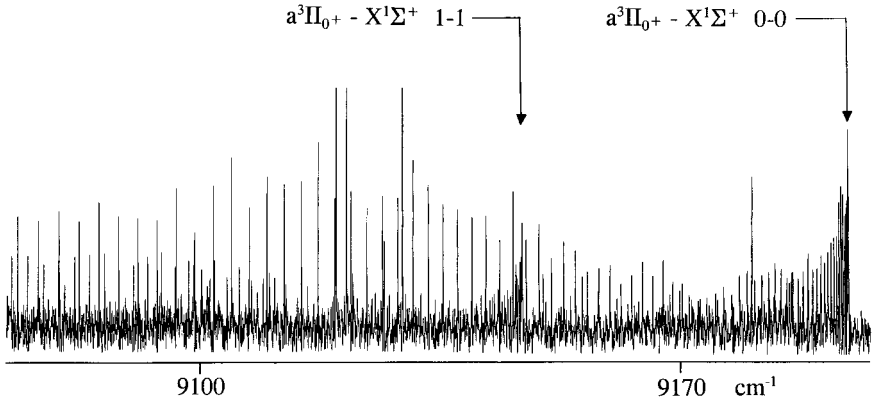

FIG. 2. A compressed portion of the 0–0 and 1–1 bands of the $a^3\Pi_0$–$X^1\Sigma^+$ system of IrN.

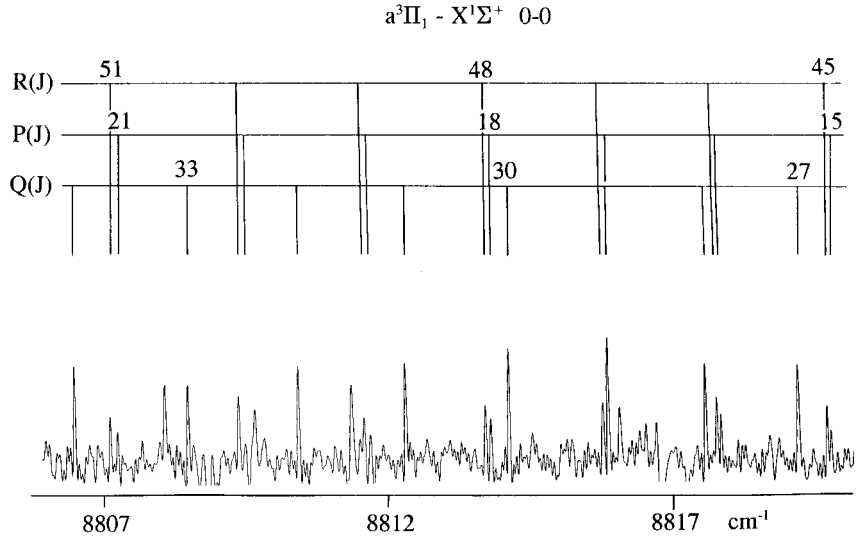

FIG. 3. An expanded portion of the 0–0 band of the $a^3\Pi_1$–$X^1\Sigma^+$ system of IrN.

orbitals. For the sake of uniformity, a similar pseudo-potential and the corresponding basis set was used for the nitrogen atom (*29*). The iridium atom basis set was augmented by a single *f* Gaussian orbital, with an exponent of 0.8, and a single *d* polarization function, with an exponent of 0.8, was added on nitrogen. The size of the CASSCF (CMRCI) wavefunctions ranged between 1200 and 1300 (170 000 and 310 000) configuration state functions (C_{2v} symmetry), depending on the space and spin symmetries. We refer to our RuN work (*24*) for more details on the computational procedure that we just summarize here.

All calculations were performed with the MOLPRO program package (*30*), running on the Cray J916 computer at the ULB/VUB computer center.

OBSERVATIONS

In our recent study of RuN (*24*) we have noted that the electronic structure of RuN is very similar to that of the isoelectronic RhC (*31*, *32*) and we expected a similar correspondence between IrN and PtC. Because no previous observations of IrN were reported below 1 μm and no theoretical calculations were available to guide us in the search for IrN transitions in the near infrared, we used the isoelectronic PtC (*19–22*) molecule as a guide. A comparison of the known electronic states of IrN and PtC indicates that the $A'\ ^1\Pi$ and $A^1\Pi$ states are observed for both IrN and PtC. For PtC, an additional low-lying transition labeled as $A''\ ^1\Sigma^+$–$X^1\Sigma^+$ was reported near 1 μm (*21*), suggesting that a similar transition could be found for IrN. We have observed several new IrN bands in the 7500–9200 cm^{-1} region, which were classified into two transitions, one with $\Delta\Omega = 0$ and the other with $\Delta\Omega = 1$. A rotational analysis indicates that these two transitions have a common lower state which is the ground state of IrN. An updated schematic energy level diagram of the observed electronic transitions of IrN is presented in Fig. 1, where the observed electronic states of the isoelectronic PtC were also provided for comparison. The two new transitions were assigned as the $^3\Pi_0$–$X^1\Sigma^+$ and $^3\Pi_1$–$X^1\Sigma^+$ subbands of the $a^3\Pi$–$X^1\Sigma^+$ transition and this assignment is supported by our *ab initio* calculations. The branches in different bands were picked out using an interactive color Loomis–Wood program running on a PC computer, which was particularly helpful in finding the weaker lines of the minor isotopomer, ^{191}IrN.

(A) The $a^3\Pi_0$–$X^1\Sigma^+$ Transition

The 0–0 band of the $^3\Pi_0$–$X^1\Sigma^+$ transition has an *R* head at 9194.3 cm^{-1}. This band is the strongest in intensity, while the 1–1 band with an *R* head at 9146.8 cm^{-1} has about 40% of the intensity of the 0–0 band. The 2–2 and other higher vibrational bands of this sequence are too weak for identification and analysis. The bands in the 0–1 sequence were also identified with the help of the known ground state molecular parameters from the previous study (*15*). The bands with *R* heads at 8083.1, 8048.2, 8015.4, 7984.4, and 7954.8 cm^{-1} were identified as the 0–1, 1–2, 2–3, 3–4, and 4–5 bands of the $a^3\Pi_0$–$X^1\Sigma^+$ transition. A search for the 1–0 sequence bands was unsuccessful partly due to the poor response of the InSb detector near 10 000 cm^{-1} where these bands are expected. The 0–2 or 2–0 sequence bands were also not observed because of their very weak intensity. A rotational analysis of the 0–0, 1–1, 0–1, 1–2, 2–3, and 3–4 bands was obtained. The rotational structure of each band of this transition consists of only two branches, one

TABLE 1

Observed Line Positions (in cm^{-1}) for the $a^3\Pi$–$X^1\Sigma^+$ System of ^{193}IrN

J	R(J)	O-C	P(J)	O-C	R(J)	O-C	P(J)	O-C	R(J)	O-C	P(J)	O-C
	$a^3\Pi_0$ - $X^1\Sigma^+$, 0 - 0				$a^3\Pi_0$ - $X^1\Sigma^+$, 1 - 1				$a^3\Pi_0$ - $X^1\Sigma^+$, 0 - 1			
4							9130.261	18				
5							9129.119	19				
6							9127.917	-2			8061.793	-4
7	9188.400	-7	9174.020	-7			9126.719	18	8074.991	-4	8060.618	2
8	9189.059	-1	9172.751	-11			9125.447	3	8075.699	-1	8059.392	-10
9	9189.672	-2	9171.449	-10	9142.252	10	9124.144	-4	8076.369	-4	8058.163	4
10	9190.260	10	9170.112	-8	9142.806	-7	9122.810	-5	8077.010	-3	8056.879	-3
11	9190.790	2	9168.745	4	9143.349	3	9121.443	-1	8077.622	-0	8055.579	4
12	9191.287	-0	9167.315	-9	9143.837	-3	9120.036	1	8078.200	1	8054.221	-15
13	9191.751	2	9165.858	-11	9144.299	3	9118.598	10	8078.745	1	8052.862	-3
14	9192.173	1	9164.375	-2			9117.111	8	8079.252	-4	8051.458	-4
15	9192.555	-0	9162.845	-0	9145.088	-6	9115.589	9	8079.729	-8	8050.019	-9
16	9192.901	-1	9161.281	5	9145.443	8	9114.026	7	8080.188	1	8048.564	3
17	9193.199	-10	9159.669	0	9145.741	3	9112.427	8	8080.607	3	8047.061	-2
18	9193.462	-16	9158.021	-3	9146.003	1	9110.797	14	8080.990	2	8045.531	-3
19	9193.697	-11	9156.333	-7	9146.239	10	9109.110	2	8081.332	-9	8043.965	-8
20	9193.897	-3	9154.623	5	9146.411	-6	9107.396	1			8042.380	-1
21	9194.045	-9	9152.860	1			9105.642	-2	8081.947	-4	8040.764	8
22	9194.165	-3	9151.065	4			9103.854	-2	8082.200	-7	8039.093	-7
23	9194.242	-2	9149.232	7			9102.032	3	8082.435	2		
24	9194.289	7	9147.355	4			9100.168	4	8082.613	-12	8035.698	5
25	9194.289	8	9145.443	5	9146.789	8	9098.263	3	8082.776	-10	8033.930	-12
26	9194.242	0	9143.494	6	9146.730	-9	9096.325	5	8082.914	0	8032.166	6
27	9194.165	1	9141.503	4	9146.663	4	9094.345	3	8082.994	-16		
28	9194.045	-2	9139.482	9	9146.542	2	9092.325	-1	8083.075	2		
29	9193.897	6	9137.416	8			9090.271	-0	8083.103	-3		
30	9193.697	0	9135.311	5	9146.181	-4	9088.172	-7	8083.103	-2		
31	9193.462	-2	9133.168	4	9145.937	-14	9086.052	4	8083.075	3		
32	9193.199	6	9130.992	6	9145.681	4	9083.884	4	8082.994	-12		
33	9192.887	6	9128.772	4	9145.356	-10	9081.675	1	8082.914	5		
34	9192.539	7	9126.520	7	9145.020	5	9079.440	10	8082.776	-3	8016.772	13
35	9192.151	7	9124.223	5	9144.629	4	9077.152	4	8082.610	-7	8014.686	-6
36	9191.722	5	9121.892	5	9144.202	4	9074.826	-2	8082.435	12	8012.583	-10
37	9191.265	15	9119.521	4	9143.718	-13	9072.476	5	8082.200	5	8010.467	5
38	9190.746	1	9117.111	2	9143.236	10	9070.079	5	8081.947	11	8008.301	2
39	9190.198	-4	9114.665	2	9142.681	-2	9067.640	-1	8081.638	-6		
40	9189.613	-6	9112.181	3	9142.100	-0	9065.167	-3	8081.332	12	8003.877	-2
41	9188.993	-4	9109.658	3			9062.656	-5	8080.958	-5	8001.634	12
42	9188.331	-4	9107.094	-0	9140.829	9	9060.115	2	8080.580	7	7999.328	-4
43	9187.629	-6	9104.496	2	9140.118	-4	9057.522	-6	8080.155	4	7997.013	2
44	9186.894	-2	9101.856	-1	9139.390	6	9054.895	-10	8079.698	1	7994.661	3
45	9186.115	-2	9099.183	2	9138.611	2			8079.209	0	7992.274	1
46	9185.295	-4	9096.464	-3	9137.805	12	9049.541	-4	8078.687	-2	7989.845	-12
47	9184.438	-4	9093.712	-3	9136.926	-14	9046.792	-16	8078.130	-6	7987.406	-2
48	9183.540	-5	9090.921	-3	9136.040	-8	9044.024	-9	8077.549	-2	7984.934	5
49	9182.612	1	9088.094	-1	9135.121	5	9041.209	-12	8076.935	2	7982.415	-2
50	9181.629	-6	9085.223	-5	9134.152	6	9038.373	3	8076.284	3	7979.863	-10
51	9180.623	2	9082.320	-2			9035.489	7	8075.599	1	7977.301	3
52	9179.564	-4	9079.368	-9	9132.080	-9	9032.541	-14	8074.873	-8	7974.699	8
53	9178.476	2	9076.390	-5	9130.992	-10	9029.603	12	8074.132	1	7972.056	4
54	9177.339	-3	9073.367	-6	9129.898	22	9026.601	12	8073.355	6	7969.380	-0
55	9176.165	-5	9070.310	-4	9128.700	-11	9023.544	-4			7966.678	0
56	9174.952	-6	9067.213	-4	9127.503	-4	9020.478	8	8071.683	-2	7963.934	-10
57	9173.699	-8	9064.075	-5	9126.278	14	9017.356	2	8070.812	8	7961.163	-14
58	9172.419	3	9060.898	-7	9124.980	-2	9014.181	-19	8069.890	0	7958.393	14
59	9171.096	10			9123.658	-2	9010.999	-9	8068.946	4		
60	9169.718	3			9122.294	-6			8067.961	0	7952.690	4
61	9168.310	5			9120.902	2			8066.948	1	7949.795	3
62	9166.857	3			9119.453	-9					7946.861	-4
63	9165.376	11							8064.832	13		
64	9163.832	-3							8063.711	5		
65	9162.281	15							8062.571	12		
66									8061.376	-3		
67									8060.165	0		

TABLE 1—*Continued*

J	R(J)	O-C	P(J)	O-C	R(J)	O-C	P(J)	O-C	R(J)	O-C	P(J)	O-C
	$a^3\Pi_0 - X^1\Sigma^+$, 1 - 2				$a^3\Pi_0 - X^1\Sigma^+$, 2 - 3				$a^3\Pi_0 - X^1\Sigma^+$, 3 - 4			
3	8037.048	-10							7973.337	4		
4	8037.882	-2							7974.146	-4		
5	8038.666	-12					7995.516	9	7974.943	8		
6	8039.444	4					7994.375	2	7975.676	-12		
7	8040.164	-7					7993.227	19	7976.422	11		
8	8040.879	8					7992.025	13	7977.102	-2		
9	8041.535	-3					7990.769	-16	7977.776	12	7959.895	-12
10	8042.165	-9					7989.528	2	7978.400	7	7958.658	-0
11	8042.769	-9							7978.997	5	7957.378	0
12	8043.351	0					7986.918	3	7979.557	-3	7956.061	-6
13	8043.890	-1					7985.565	2	7980.096	-0	7954.719	-5
14	8044.402	2			8011.607	-3	7984.179	-0	7980.600	-1	7953.356	4
15	8044.862	-14			8012.088	2	7982.757	-8	7981.086	11	7951.947	-1
16	8045.316	-6	8013.897	-9	8012.521	-8	7981.325	6	7981.516	-2	7950.524	10
17					8012.938	-4			7981.938	8	7949.050	1
18	8046.119	2	8010.892	-6	8013.319	-5	7978.335	1	7982.306	-4	7947.549	-3
19	8046.462	-5	8009.335	-11	8013.669	-4	7976.791	-4	7982.665	6	7946.026	0
20	8046.770	-15	8007.764	1			7975.221	-3	7982.980	2	7944.465	-3
21	8047.064	-7	8006.145	-3			7973.627	4	7983.260	-4	7942.873	-6
22	8047.316	-10	8004.506	3	8014.550	17	7971.987	-3	7983.519	-1	7941.268	9
23	8047.548	-0	8002.831	6					7983.747	3	7939.603	-6
24	8047.729	-9	8001.113	-4			7968.637	6	7983.937	-0		
25	8047.886	-11	7999.372	-5	8015.097	-12	7966.900	-6	7984.101	2		
26	8048.025	1	7997.611	6	8015.257	19	7965.143	-6			7934.468	-5
27	8048.112	-6	7995.804	2	8015.339	4	7963.364	3	7984.330	2	7932.714	15
28	8048.185	4	7993.964	-4			7961.541	-0	7984.408	12	7930.892	-3
29	8048.211	-1	7992.097	-5	8015.438	4	7959.697	6	7984.439	6	7929.057	-3
30	8048.211	0	7990.206	1	8015.438	2	7957.808	-2	7984.439	1	7927.199	5
31	8048.185	7	7988.271	-5	8015.408	1	7955.895	-2	7984.408	-3	7925.291	-7
32	8048.112	-0	7986.318	2	8015.339	-7	7953.953	-1	7984.351	-2	7923.362	-8
33	8048.025	9	7984.332	8	8015.257	4	7951.972	-7	7984.255	-9	7921.408	-4
34	8047.886	-1	7982.306	4	8015.128	-1	7949.983	9			7919.415	-7
35	8047.729	4	7980.243	-5	8014.977	5	7947.940	3	7984.002	12	7917.402	-1
36	8047.548	15	7978.165	3	8014.785	1	7945.873	4	7983.809	3	7915.347	-5
37	8047.316	9	7976.051	6	8014.552	-13			7983.596	5	7913.268	-2
38	8047.064	15	7973.895	-3	8014.312	-1	7941.640	-1	7983.334	-9	7911.145	-13
39	8046.770	10	7971.726	8	8014.012	-18	7939.478	-2	7983.071	6		
40	8046.438	-0	7969.510	3	8013.709	-5			7982.757	2	7906.846	5
41	8046.090	6	7967.269	5	8013.357	-10	7935.064	-2	7982.415	2	7904.636	-0
42	8045.689	-9	7964.996	5	8012.989	0	7932.810	-2	7982.051	11		
43	8045.268	-12	7962.686	0	8012.583	5	7930.517	-10	7981.640	5	7900.132	-2
44			7960.355	6	8012.147	12	7928.212	1	7981.204	6		
45	8044.339	-8	7957.979	-3	8011.668	7	7925.866	1	7980.730	1		
46	8043.824	-8	7955.580	-3	8011.138	-17	7923.488	1	7980.243	14		
47	8043.282	-2	7953.154	1			7921.082	5	7979.690	-7		
48	8042.699	-6	7950.700	9	8010.051	5	7918.634	-4	7979.130	-4		
49	8042.090	-3	7948.200	2	8009.446	2	7916.166	-1	7978.536	-2		
48			7945.668	-5	8008.792	-17	7913.663	-2	7977.909	-1		
51	8040.764	-9	7943.129	11					7977.248	-3		
52	8040.072	8	7940.530	-1			7908.562	-6	7976.555	-6		
53	8039.321	-2										
54	8038.545	-5	7935.250	-13					7975.088	6		
55	8037.752	7	7932.588	6			7900.689	-2	7974.298	3		
56	8036.915	9	7929.863	-7					7973.477	0		
57	8036.026	-10	7927.129	3					7972.626	-0		
58	8035.125	-7	7924.352	1								
59	8034.213	16	7921.543	-2								
60	8033.244	15	7918.702	-5								
61	8032.235	7	7915.845	7								
62	8031.209	14	7912.939	1								
63	8030.135	6	7910.005	-1								
64			7907.043	0								
65			7904.042	-7								
66			7901.026	3								

TABLE 1—*Continued*

J	R(J)	O-C	P(J)	O-C	Q(J)	O-C	R(J)	O-C	P(J)	O-C	Q(J)	O-C
	$a^3\Pi_1 - X^1\Sigma^+$, 0 - 0						$a^3\Pi_1 - X^1\Sigma^+$, 0 - 1					
6	8846.484	-3			8840.026	1					7726.557	-13
7	8846.974	-12			8839.606	-11					7726.191	-15
8	8847.425	2									7725.772	-18
9	8847.797	1			8838.622	-3						
10	8848.105	-3			8838.036	-6					7724.807	3
11			8826.850	-13	8837.397	-2					7724.215	-18
12	8848.539	-6			8836.698	-1					7723.608	-2
13	8848.676	7	8823.432	-7	8835.937	-3					7722.942	8
14	8848.742	10	8821.631	-2	8835.122	-1					7722.217	9
15	8848.742	10	8819.761	-6	8834.244	-3					7721.439	10
16	8848.676	7	8817.829	-7	8833.316	3					7720.601	3
17	8848.539	-6	8815.854	9	8832.322	1					7719.708	-7
18			8813.785	-7	8831.276	7					7718.786	6
19	8848.105	-3	8811.675	-1	8830.164	4	7735.742	1	7699.299	-11	7717.789	-5
20	8847.797	1	8809.495	-3			7735.564	5	7697.252	-8	7716.756	1
21	8847.425	3	8807.259	1	8827.773	6	7735.320	0	7695.149	-7	7715.673	9
22	8846.974	-11	8804.953	-3	8826.488	6	7735.022	-2	7692.989	-7	7714.530	9
23	8846.484	-2	8802.587	-6	8825.142	4	7734.664	-10			7713.331	5
24	8845.905	-19	8800.170	3	8823.744	8			7688.514	4	7712.077	-2
25	8845.301	2	8797.680	1	8822.284	8	7733.813	9	7686.186	3	7710.777	-4
26	8844.612	-1	8795.127	-2	8820.768	10	7733.283	-2	7683.795	-6	7709.435	5
27	8843.861	-3	8792.508	-9	8819.188	7			7681.353	-11	7708.039	12
28	8843.058	6	8789.833	-11	8817.554	8	7732.078	-1	7678.862	-9	7706.565	-7
29	8842.183	5	8787.099	-9	8815.854	3			7676.330	7	7705.062	-3
30	8841.246	4	8784.301	-10	8814.105	7	7730.654	5	7673.704	-14	7703.509	3
31	8840.252	9	8781.460	9	8812.295	7	7729.852	2	7671.061	2	7701.906	11
32	8839.184	2	8778.528	-2	8810.424	6	7729.011	16	7668.348	4	7700.239	7
33	8838.061	4	8775.555	8	8808.493	4	7728.085	0	7665.572	-2	7698.516	-1
34	8836.878	7	8772.500	-2	8806.506	3	7727.106	-11	7662.763	14	7696.754	4
35	8835.618	-4			8804.459	2	7726.080	-15	7659.879	11	7694.936	6
36	8834.322	12			8802.357	4			7656.933	2	7693.062	4
37	8832.940	5			8800.187	-3			7653.941	1	7691.131	-4
38	8831.513	14			8797.968	-0			7650.885	-7	7689.158	-1
39	8830.004	4	8756.353	5	8795.687	-2			7647.780	-10	7687.140	9
40	8828.450	12	8752.929	-2	8793.350	0			7644.637	4	7685.051	0
41	8826.837	24	8749.449	-5	8790.945	-8					7682.915	-4
42	8825.142	15	8745.908	-6	8788.492	-4			7638.145	-7	7680.730	-4
43	8823.374	-3	8742.304	-8	8785.977	-5			7634.818	-10	7678.497	-0
44	8821.564	-1	8738.641	-8	8783.401	-7					7676.212	3
45	8819.691	-0	8734.913	-11	8780.767	-8			7628.005	-11	7673.863	-4
46	8817.756	3							7624.516	-10	7671.478	3
47	8815.762	8							7620.972	-10	7669.025	-4
48	8813.692	0			8772.533	7			7617.367	-16	7666.522	-8
49	8811.570	4			8769.663	4			7613.727	-1	7663.970	-11
50	8809.379	-0			8766.725	-7			7610.017	-2	7661.376	-2
51	8807.128	-1							7606.261	6	7658.731	7
52	8804.816	-0			8760.694	-8			7602.432	-2	7656.010	-6
53	8802.438	-3			8757.606	6			7598.568	8	7653.252	-5
54	8800.002	-1			8754.434	-4			7594.624	-6	7650.454	10
55	8797.502	-1			8751.219	2			7590.652	7	7647.577	-4
56	8794.940	1			8747.938	1			7586.612	8	7644.662	-2
57	8792.323	10			8744.591	-7					7641.692	-3
58	8789.624	-0			8741.205	5					7638.675	1
59	8786.875	2			8737.734	-9					7635.590	-9
60	8784.059	-0			8734.233	6					7632.476	3
61	8781.174	-9			8730.646	-6						
62					8727.031	13						
63					8723.314	-10						
64					8719.580	8						
65					8715.760	-0						
66					8711.901	12						
67					8707.956	-3						
68					8703.983	13						

R and one *P*, consistent with a $\Delta\Omega = 0$ transition. A portion of the spectrum of the $a^3\Pi_0$–$X^1\Sigma^+$ subband of IrN is presented in Fig. 2, where the *R* heads of the 0–0 and 1–1 bands were marked. The lines belonging to the minor isotopomer ^{191}IrN were also identified in our spectra but the molecular constants were determined only for the most abundant ^{193}IrN isotopomer.

TABLE 1—*Continued*

J	R(J)	O-C	P(J)	O-C	Q(J)	O-C	J	R(J)	O-C	P(J)	O-C	Q(J)	O-C
						$a^3\Pi_1$ - $X^1\Sigma^+$, 1 - 2							
9					7608.693	2	28	7615.617	8			7589.994	-0
10					7608.177	3	29	7614.944	5			7588.491	-0
11					7607.599	-6	30	7614.215	1			7586.933	-3
12					7606.977	-7	31	7613.432	-2			7585.328	-1
13					7606.321	11	32	7612.612	13			7583.676	5
14			7592.245	-3	7605.582	-3	33					7581.951	-9
15			7590.478	-18	7604.804	-5	34	7610.762	1			7580.203	5
16	7619.333	-1	7588.681	-7	7603.976	-5	35	7609.750	-8			7578.389	6
17	7619.333	6	7586.819	-7	7603.100	0	36	7608.691	-9	7541.031	-5	7576.513	-3
18	7619.259	-7	7584.906	-3	7602.174	6	37	7607.589	2	7538.083	5	7574.597	0
19	7619.157	8	7582.959	21	7601.189	5	38	7606.433	14	7535.078	13	7572.633	7
20	7618.996	20	7580.916	5	7600.147	-2	39	7605.189	-5	7532.012	13	7570.600	-2
21	7618.753	4	7578.824	-6	7599.055	-6	40	7603.907	-7	7528.892	16	7568.523	-4
22	7618.466	0	7576.713	19	7597.916	-5	41	7602.572	-7	7525.707	8	7566.397	-2
23	7618.130	2	7574.504	1	7596.741	11	42	7601.189	0	7522.469	1		
24	7617.732	-3	7572.270	12	7595.492	6	43	7599.734	-8	7519.169	-13		
25	7617.287	1	7569.941	-15	7594.190	-1	44	7598.249	9	7515.854	14		
26	7616.779	-4	7567.599	-2	7592.847	2	45	7596.669	-13	7512.439	-6		
27	7616.228	4			7591.443	-3	46	7595.078	10				

Note: O-C are observed minus calculated line positions in the units of 10^{-3} cm^{-1}.

(B) The $a^3\Pi_1$–$X^1\Sigma^+$ Transition

On the lower wavenumber side of the $a^3\Pi_0$–$X^1\Sigma^+$ 0–0 band, another band was observed with a 0–0 *R* head at 8848.9 cm^{-1}. This band involves a $\Delta\Omega = 1$ transition with the ground state $v = 0$ vibrational level as its lower state. We have assigned this band as the 0–0 band of the $a^3\Pi_1$–$X^1\Sigma^+$ subband. The expected position of the 1–1 band is overlapped by a very strong atomic line with extensive ringing, and therefore, the rotational structure could not be measured. The 2–2 or other higher vibrational bands of this sequence were also not identified because of their very weak intensity. The 0–1 and 1–2 bands of this subband were identified using the ground state vibrational intervals obtained from the analysis of the $A^1\Pi$–$X^1\Sigma^+$ and $A'\ ^1\Pi$–$X^1\Sigma^+$ transitions (*15*). A rotational analysis of the 0–0, 0–1, and 1–2 bands of this subband were carried out. Each band of this subband has three branches, one *P*, one *Q*, and one *R* with the *Q* branch being the most intense. The *R* and *P* branches appear with similar intensity. A portion of the 0–0 band of this transition is presented in Fig. 3 with the *P*, *Q* and *R* branches marked.

RESULTS

While obtaining the vibrational assignment of the near-infrared bands of IrN, we noted that the excited state vibra-

TABLE 2
Molecular Constants (in cm^{-1}) for the $X^1\Sigma^+$, $a^3\Pi_0$, and $a^3\Pi_1$ States of ^{193}IrN from an Empirical Fit

State	Const.	v=0	v=1	v=2	v=3	v=4
$X^1\Sigma^+$	T_v	0.0	1113.59138(40)	2214.58779(59)	3302.9747(12)	4378.7445(13)
	B_v	0.4984986(24)	0.4952772(24)	0.4920300(25)	0.4887623(28)	0.4854760(30)
	$D_v \times 10^7$	3.9566(46)	3.9918(49)	4.0220(48)	4.0558(67)	4.1045(72)
$a^3\Pi_0$	T_v	9181.80718(60)	10248.02538(73)	11303.6825(16)	12348.5040(15)	--
	B_v	0.4793972(24)	0.4762262(26)	0.4731175(36)	0.4699910(33)	--
	$D_v \times 10^7$	4.1724(48)	4.0931(52)	4.122(11)	4.2229(82)	--
$a^3\Pi_1$	T_v	8841.25142(73)	9825.6087(21)	--	--	--
	B_v	0.4683470(25)	0.4653540(55)	--	--	--
	$D_v \times 10^7$	4.0203(51)	4.176(26)	--	--	--
	$q_v \times 10^3$	-1.9410(10)	-1.5946(42)	--	--	--
	$q_{Dv} \times 10^8$	2.033(35)	0.87(32)	--	--	--

Note: Numbers in parentheses are one standard deviation uncertainty in the last digits.

TABLE 3
Molecular Constants (in cm^{-1}) for the $X^1\Sigma^+$ and $a^3\Pi$ States of ^{193}IrN from the Case (a) Fit of the $a^3\Pi$ State

State	Const.[a,b]	v=0	v=1	v=2
$X^1\Sigma^+$	T_v	0.0	1113.59132(42)	2214.58779(60)
	B_v	0.49849844(77)	0.49527702(76)	0.49202967(90)
	$D_v \times 10^7$	3.9610(20)	3.9962(21)	4.0259(23)
$a^3\Pi$	T_v	8840.31747(88)	9824.6804(21)	--
	A_v	-340.53329(93)	-422.3959(22)	--
	$A_{Dv} \times 10^3$	-9.6718(15)	-9.7513(72)	--
	B_v	0.46840868(94)	0.4654029(49)	--
	$D_v \times 10^7$	4.0421(23)	4.184(25)	--
	$q_v \times 10^3$	1.9865(11)	1.6436(59)	--
	$q_{Dv} \times 10^8$	-5.561(65)	-7.10(75)	--
	$p_v \times 10^5$	-1.125(12)	-1.78(11)	--

[a]See text for details.
[b]Numbers in parentheses are one standard deviation uncertainty in the last digits.

tional intervals of the $a^3\Pi_0$ and $a^3\Pi_1$ spin components are considerably different, indicating an interaction of the $a^3\Pi$ state with the other nearby states. The rotational analysis of both subbands was initially obtained by treating the two excited spin components as separate states. Since both subbands involve the ground state as their common lower state, the rotational assignments in different bands were accomplished by comparing the lower state combination differences to the values obtained in our previous study of the $A^1\Pi$–$X^1\Sigma^+$ and $A'\ ^1\Pi$–$X^1\Sigma^+$ transitions (*15*). The rotational constants were determined by fitting the observed line positions of the two subbands to the customary empirical energy level expressions:

$$F_v(J) = T_v + B_vJ(J+1) - D_v[J(J+1)]^2 + H_v[J(J+1)]^3 \quad [1]$$

$$F_v(J) = T_v + B_vJ(J+1) - D_v[J(J+1)]^2 + H_v[J(J+1)]^3 \pm 1/2\{qJ(J+1) + q_D[J(J+1)]^2\}. \quad [2]$$

In the final fit the blended lines were given reduced weights. The lines overlapped by N_2 molecular lines or strong atomic lines were excluded. In the final fit, the lines of both subbands were combined with the lines of the $A^1\Pi$–$X^1\Sigma^+$ and $A'\ ^1\Pi$–$X^1\Sigma^+$ transitions (*15*) and a global fit was obtained to determine a single set of molecular constants for each vibrational level. The observed line positions of the $a^3\Pi_0$–$X^1\Sigma^+$ and $a^3\Pi_1$–$X^1\Sigma^+$ subbands are provided in Table 1 and the molecular constants obtained for the $X^1\Sigma^+$, $a^3\Pi_0$, and $a^3\Pi_1$ states of ^{193}IrN are provided in Table 2.

At the final stage of the analysis, we tried to combine the two subbands in order to obtain a Hund's case (a) fit for the excited $a^3\Pi$ state. Initially the lines of only the 0–0, 1–1, 0–1, and 1–2 bands were included since the $v = 0$ and 1 vibrational levels were observed in both $a^3\Pi_0$–$X^1\Sigma^+$ and $a^3\Pi_1$–$X^1\Sigma^+$ transitions. The observed transition wavenumbers were fitted with the usual N^2 Hamiltonian for the $^3\Pi$ state as given by Brown *et al.* (*33*). An explicit listing of the $^3\Pi$ state matrix elements is provided by Brazier *et al.* (*34*). In this fit the molecular constants T_v, A_v, A_{Dv}, B_v, D_v, q_v, q_{Dv}, and p_v were determined with the standard deviation of fit of 0.95. The spectroscopic constants such as A_v are only effective values because we are missing the $^3\Pi_{0^-}$ and $^3\Pi_2$ spin components. The inclusion of the 2–3 and 3–4 bands, which were observed only for the $a^3\Pi_0$–$X^1\Sigma^+$ subband, caused a deterioration in the quality of the fit so that we decided not to include these bands. The constants obtained from the case (a) fit of the 0–0, 1–1, 0–1, and 1–2 bands are provided in Table 3. The constants of Table 3 are very much affected by global interaction with other states and this results in, for example, very strong vibrational dependence of constant *A*.

AB INITIO RESULTS

The potential energy curves calculated at the CMRCI level of theory are shown in Figs. 4 and 5 for the singlet and triplet spin manifolds, respectively. The energy scale used in these figures is relative to the minimum energy of the ground $X^1\Sigma^+$

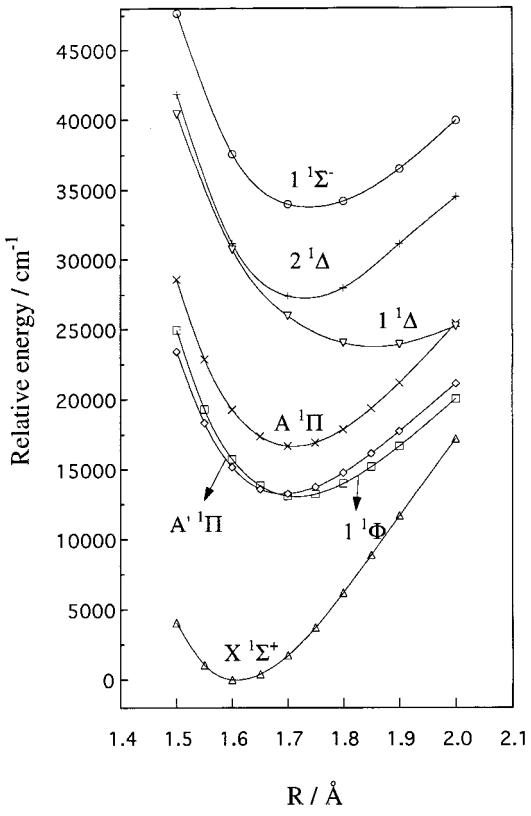

FIG. 4. The low-lying singlet potential energy curves of IrN, from CMRCI calculations.

electronic state. The low-lying excited states in the singlet system are, in order of increasing term energy: $1^1\Phi$, $A'\ ^1\Pi$, $A^1\Pi$, $1^1\Delta$, $2^1\Delta$, and $1^1\Sigma^-$. The energy ordering within the triplet system is the following: $a^3\Pi$, $b^3\Phi$, $c^3\Pi$, $1^3\Sigma^+$, $1^3\Delta$, $1^3\Sigma^-$, and $2^3\Delta$. The relative energy scale between both spin systems is better illustrated in Fig. 6.

The correlation diagram drawn in Fig. 7 allows an interepretation of the electronic state ordering predicted by our CMRCI calculations. This figure correlates the molecular orbitals of IrN to those of the iridium and nitrogen atoms in their ground states. This diagram was obtained from size-consistent full-valence CASSCF calculations performed on the different species: IrN, Ir(^{4}F), and N(^{4}S). The IrN orbitals were obtained from a state-averaged CASSCF calculation performed, at an internuclear distance of 1.6 Å, on the singlet states correlating to the ground dissociation channel Ir(^{4}F) + N(^{4}S), i.e., the $X^1\Sigma^+$, $1^1\Phi$, $A'\ ^1\Pi$, and $1^1\Delta$ states. One can verify in Fig. 4 that these states do converge to the same dissociation limit at large internuclear distances. Figure 7 provides a helpful one-electron picture for discussing the electronic structure of IrN. Note that we have chosen to label only the valence orbitals. The dotted lines connecting the orbitals of IrN to those of the atomic dissociation products give qualitative information on the LCAO content of the molecular orbitals, as provided by the analysis of the CASSCF wavefunctions. One finds that

(i) The 2σ and 3σ MOs are, respectively, constructed from bonding and antibonding combinations of $5d\sigma$(Ir) and $2p\sigma$(N).

(ii) 3σ has, in addition, some of the $6s\sigma$(Ir)–$2p\sigma$(N) bonding character.

(iii) 1π and 2π, respectively, come from bonding and antibonding combinations of $5d\pi$(Ir) and $2p\pi$(N).

(iv) 4σ is the antibonding analog of 3σ.

This orbital analysis is quite similar to the one obtained for RuN using the same computational approach (*24*), and both nitrides have similar correlation diagrams (see Fig. 7 of Ref. (*24*)). The major difference to be stressed is the smaller 2π–4σ energy gap in IrN (0.11 hartrees) than in RuN (0.22 hartrees) coming from a more antibonding 2π orbital in IrN. It follows, as discussed below, that single electron promotions to the 2π and 4σ orbitals need to be considered in IrN.

The electron orbital filling represented on Fig. 7, with the 14 valence electrons distributed in the low-lying orbitals, confirms the ground configuration as (*15*):

$$1\sigma^2 2\sigma^2 1\pi^4 1\delta^4 3\sigma^2 \quad (X^1\Sigma^+).$$

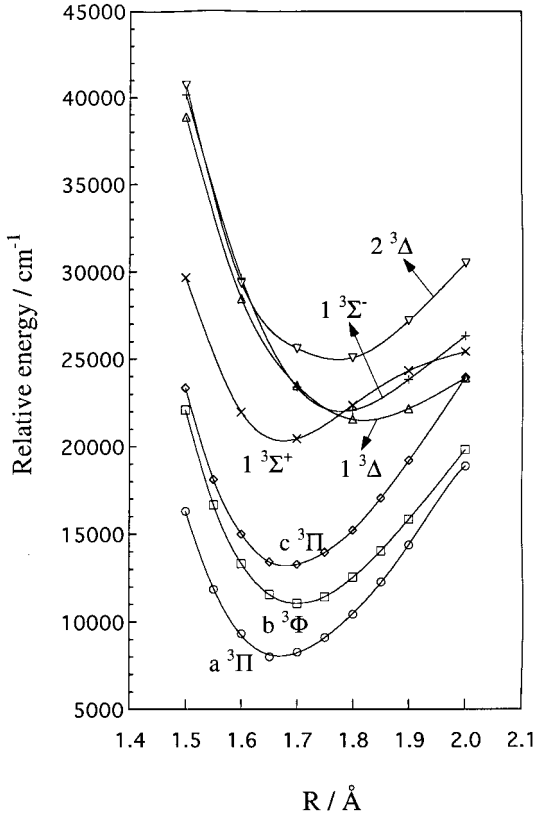

FIG. 5. The low-lying triplet potential energy curves of IrN, from CMRCI calculations.

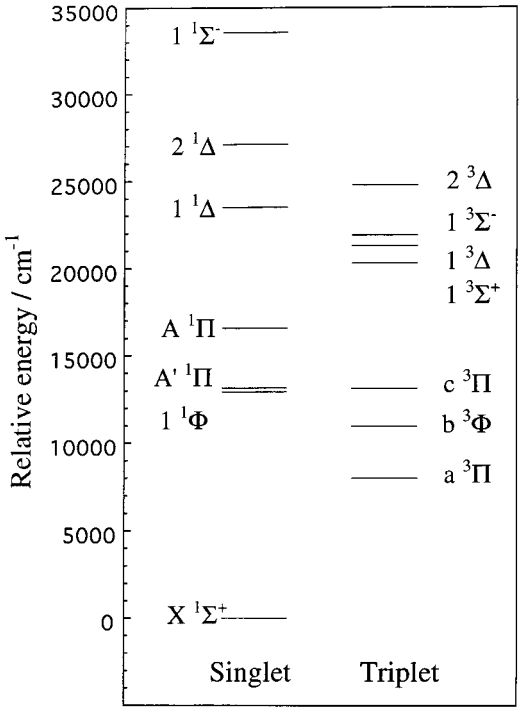

FIG. 6. Relative energies within the singlet and triplet systems of IrN, from CMRCI calculations.

This prediction is in agreement with the analysis of the corresponding CMRCI wavefunctions provided in Table 4 for the singlet states. This table lists the main configurations contributing to the CI expansions, together with their weights in the wavefunctions. The configuration weights are given by the square of the corresponding CI coefficients. One sees that configuration $1\sigma^2 2\sigma^2 1\pi^4 1\delta^4 3\sigma^2$ contributes 76% to the ground state wavefunction. All singlet states are characterized by a single dominant configuration. The weight of these configurations, however, only ranges between 70 and 80%. The weight of any single secondary configuration is quite small and the remaining contributions to the wavefunction are distributed over a large number of configurations. These features demonstrate the existence of strong electron correlation effects, already observed in RuN (*24*). Table 5 provides similar information for the triplet manifolds. Configuration mixing is more pronounced in the triplet system, as further discussed below.

The electronic structure of the 14 states calculated in this work can be explained in terms of eight leading configurations reported in Table 6 together with the corresponding electron promotions with respect to the ground configuration (see Fig. 7). These configurations will be referred to as configurations (A) to (H), Table 4. One finds that:

(i) The singlet and triplet Π and Φ states below 20 000 cm^{-1} arise from configurations (B) and (C). As detailed in Table 5, a strong mixing between these two configurations is observed for the $^3\Pi$ states, although the corresponding $^1\Pi$ states are more pure.

(ii) Configuration (D) is the main component of the $1^1\Delta$, $1^{-1}\Sigma^-$, $1^3\Delta$, $2^3\Delta$, $1^3\Sigma^-$ states.

(iii) The $2^1\Delta$ and $1^3\Sigma^+$ states do not arise from configuration (D), but rather from configurations (E) and (F), respectively, both implying an electron promotion to the 4σ orbital.

(iv) Competition between three configurations (D, G, and H), characterized by two electron promotions to the 2π orbital, is observed for the $1^3\Sigma^-$ state.

The spectroscopic properties calculated from the CMRCI potential energy curves are given in Table 7: the equilibrium internuclear distances R_e, the harmonic frequencies at equilibrium ω_e, and the term energies T_0, corrected for the zero point energy contribution calculated within the harmonic approximation.

DISCUSSION

From our recent studies of some transition metal containing diatomic nitride molecules we have noted a remarkable resemblance in the electronic structure of nitrides and isoelectronic carbide molecules. For example, the electronic structure of RuN (*24*) is found to be very similar to that of RhC (*31*, *32*) and the electronic structure of OsN (*13*) is very similar to that

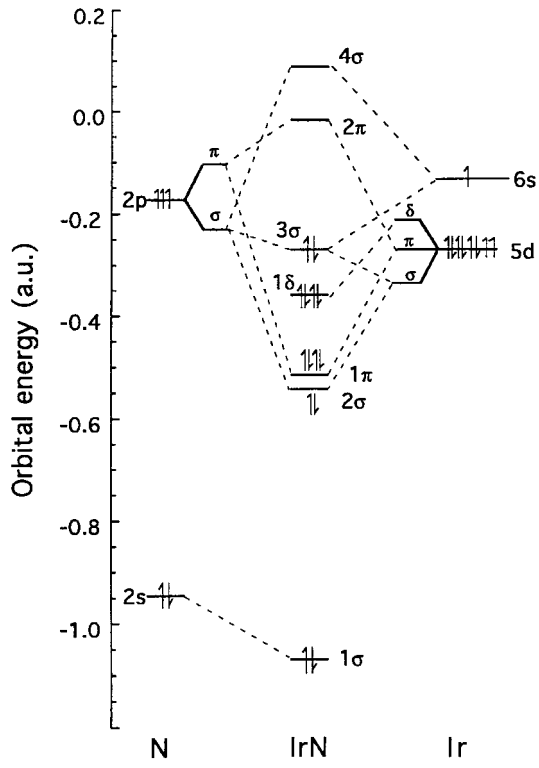

FIG. 7. The molecular orbital correlation diagram for IrN, from CASSCF calculations.

TABLE 4
Weights of the Main Configurations in the Low-Lying Singlet Electronic States of IrN from an Analysis of the CMRCI Wavefunctions

State[1]	Configuration[2]							Configuration Weights (%)[3]
	1σ	2σ	1π	1δ	3σ	2π	4σ	
$X\ ^1\Sigma^+$	2	2	4	4	2			76
	2	2	3	4	2	1		4
	2	2	2	4	2	2		4
$1\ ^1\Phi$	2	2	4	3	2	1		80
	2	2	2	3	2	3		3
$A'\ ^1\Pi$	2	2	4	4	1	1		79
	2	2	2	4	1	3		3
$A\ ^1\Pi$	2	2	4	3	2	1		79
	2	2	2	3	2	3		3
$1\ ^1\Delta$	2	2	4	3	1	2		73
	2	2	3	3	1	3		8
$2\ ^1\Delta$	2	2	4	3	2	0	1	71
	2	2	2	3	2	2	1	6
$1\ ^1\Sigma^-$	2	2	4	3	1	2		70
	2	1	4	3	2	1		5

[1] States are listed in order of energy.
[2] Molecular orbital occupancies are given in this column.
[3] Weights (in percent) are obtained from the square of the corresponding configuration interaction coefficients; configurations having weights greater than 1% are listed.

of IrC (*14*, *35*, *36*). Likewise the electronic structure of IrN is expected to be very similar to the electronic structure of isoelectronic PtC (*19–22*) (see Fig. 1). Interestingly, a similar correspondence between the oxides and nitrides does not exist for the group VIII transition metal derivatives, contrary to expectations.

So far the electronic spectra of IrN were investigated only in the 3000–20 000 cm^{-1} region. As seen in Fig. 1, there is a remarkable similarity between the low-lying $A'\ ^1\Pi$ and $A^1\Pi$ states of IrN and PtC. The two $\Omega = 1$ and $\Omega = 0$ states of IrN observed in the near-infrared region of IrN were assigned as the $^3\Pi_1$ and $^3\Pi_0$ spin components of the $a^3\Pi$ state. This assignment is also supported by our *ab initio* calculations. This work has implications for the $A''\ ^1\Sigma^+$ state of PtC. In the light of our present observations for IrN, we propose that the $A''\ ^1\Sigma^+$ state of PtC should be reassigned as the $^3\Pi_0$ spin component of the analogous $a^3\Pi$ state and that the $^3\Pi_1$ spin component lies unobserved to lower wavenumbers.

The spectroscopic constants of Table 2 were used to evaluate the equilibrium constants in the $a^3\Pi$ state. Since the $a^3\Pi_0$ and $a^3\Pi_1$ spin components have quite different spectroscopic constants, we decided to evaluate the equilibrium constants for both the spin components separately. The equilibrium constants for the $X^1\Sigma^+$, $a^3\Pi_0$ and $a^3\Pi_1$ states are provided in Table 8. As seen in this table, the $a^3\Pi_0$ and $a^3\Pi_1$ states have very different vibrational constants.

There is a very good agreement between the experimental and *ab initio* results (see Table 7). The available experimental values agree fairly well with the corresponding theoretical values, with discrepancies of about 1% for R_e, between 3 and 8% for ω_e, and less than 1400 cm^{-1} for T_0 values. For example, the $a^3\Pi$ state is predicted at 7991 cm^{-1}, compared to the observed value of 8840 cm^{-1}. The present *ab initio* results confirm the previous assignment for the $A'\ ^1\Pi$ and $A^1\Pi$ states (*15*) and the new $a^3\Pi$–$X^1\Sigma^+$ transition. No definitive information about the regular or inverted character of the $a^3\Pi$ state can be deduced from the analysis of the wavefunction, given the observed configuration mixing.

CONCLUSION

The near infrared region of IrN was investigated using a Fourier transform spectrometer. The new bands observed in the 7500–9000 cm^{-1} region were classified into two transitions

TABLE 5
Weights of the Main Configurations in the Low-Lying Triplet Electronic States of IrN from an Analysis of the CMRCI Wavefunctions

State[1]	Configuration[2]							Configuration Weights (%)[3]
	1σ	2σ	1π	1δ	3σ	2π	4σ	
a $^3\Pi$	2	2	4	4	1	1		44
	2	2	4	3	2	1		34
b $^3\Phi$	2	2	4	3	2	1		79
	2	2	2	3	2	3		4
c $^3\Pi$	2	2	4	3	2	1		66
	2	2	4	4	1	1		22
1 $^3\Sigma^+$	2	2	4	4	1	0	1	78
	2	2	2	4	1	2	1	5
1 $^3\Delta$	2	2	4	3	1	2		78
	2	2	3	3	1	3		5
1 $^3\Sigma^-$	2	2	4	3	1	2		44
	2	2	4	4	0	2		22
	2	2	4	2	2	2		12
2 $^3\Delta$	2	2	4	3	1	2		76
	2	2	3	3	1	3		2

[1] States are listed in order of energy.
[2] Molecular orbital occupancies are given in this column.
[3] Weights (in percent) are obtained from the square of the corresponding configuration interaction coefficients; configurations having weights greater than 1% are listed.

TABLE 6
Leading Configurations for the Low-Lying Electronic States of IrN

Label	Configuration	Electron promotion
(A)	$1\sigma^2\,2\sigma^2\,1\pi^4\,1\delta^4\,3\sigma^2$	
(B)	$1\sigma^2\,2\sigma^2\,1\pi^4\,1\delta^3\,3\sigma^2\,2\pi^1$	$1\delta \rightarrow 2\pi$
(C)	$1\sigma^2\,2\sigma^2\,1\pi^4\,1\delta^4\,3\sigma^1\,2\pi^1$	$3\sigma \rightarrow 2\pi$
(D)	$1\sigma^2\,2\sigma^2\,1\pi^4\,1\delta^3\,3\sigma^1\,2\pi^2$	$1\delta\,3\sigma \rightarrow 2\pi^2$
(E)	$1\sigma^2\,2\sigma^2\,1\pi^4\,1\delta^3\,3\sigma^2\,4\sigma^1$	$1\delta \rightarrow 4\sigma$
(F)	$1\sigma^2\,2\sigma^2\,1\pi^4\,1\delta^4\,3\sigma^1\,4\sigma^1$	$3\sigma \rightarrow 4\sigma$
(G)	$1\sigma^2\,2\sigma^2\,1\pi^4\,1\delta^4\,2\pi^2$	$3\sigma^2 \rightarrow 2\pi^2$
(H)	$1\sigma^2\,2\sigma^2\,1\pi^4\,1\delta^2\,3\sigma^2\,2\pi^2$	$1\delta^2 \rightarrow 2\pi^2$

TABLE 7
Spectroscopic Properties of the Low-Lying Electronic States of IrN from CMRCI *Ab Initio* Calculations

Spin multiplicity	State	T_0 (cm^{-1})	r_e (Å)	ω_e (cm^{-1})
1	$X\ ^1\Sigma+$	0	1.609	1161
			(1.6068)[a]	(1126)[a]
	$1\ ^1\Phi$	12937	1.716	898
	$A'\ ^1\Pi$	13143	1.694	961
		(13135[a]	(1.6786)[a]	(1014)[a]
	$A\ ^1\Pi$	16565	1.710	952
		(15186.7)[a]	(1.6847)[a]	(937)[a]
	$1\ ^1\Delta$	23491	1.855	635
	$2\ ^1\Delta$	27117	1.732	977
	$1^1\Sigma^-$	33562	1.740	870
3	$a\ ^3\Pi$	7991	1.673	1009
		(8840)[b]	(1.6577)[b,c]	(984)[b,d]
	$b\ ^3\Phi$	10958	1.700	971
	$c\ ^3\Pi$	13136	1.686	1014
	$1\ ^3\Sigma+$	20303	1.680	1050
	$1\ ^3\Delta$	21308	1.823	813
	$1\ ^3\Sigma^-$	21911	1.781	964
	$2\ ^3\Delta$	24786	1.770	830

Note. Experimental values are given in parentheses.
[a] Ref. (15).
[b] This work (see Table 3).
[c] r_0 value.
[d] $\Delta G(1/2)$ value.

TABLE 8
Equilibrium Constants (in cm^{-1}) for the $X^1\Sigma^+$, $a^3\Pi_0$, and $a^3\Pi_1$ States of ^{193}IrN

Const.[a]	$X^1\Sigma^+$	$a^3\Pi_0$ [b]	$a^3\Pi_1$ [b]
ω_e	1126.1757(28)	1076.5163(60)	[984.3573(23)][c]
$\omega_e x_e$	6.2889(15)	5.0747(28)	--
$\omega_e y_e$	-0.00200(22)	-0.04575(57)	--
B_e	0.5001030(22)	0.480985(26)	0.4698435(39)
$\alpha_e \times 10^3$	3.2020(22)	3.188(33)	2.9930(60)
$\gamma_e \times 10^5$	-1.080(44)	1.36(84)	--
r_e(Å)	1.6068281(35)	1.638451(45)	1.6577634(69)

[a] Numbers in parentheses are one standard deviation uncertainty in the last digits.
[b] Equilibrium constants from the case (a) constants of the $a^3\Pi$ state (Table III) are: $\Delta G(1/2)$ = 984.3629(23) cm^{-1}, B_e = 0.4699116(27) cm^{-1}, α_e = 0.0030058(50) cm^{-1}, and r_e = 1.6576432(47) Å.
[c] $\Delta G(1/2)$ value.

with 0–0 R heads at 9194.3 and 8848.9 cm^{-1}. These two transitions were assigned as $a^3\Pi_0$–$X^1\Sigma^+$ and $a^3\Pi_1$–$X^1\Sigma^+$ subbands of the $a^3\Pi$–$X^1\Sigma^+$ transition. A rotational analysis of several bands of both subbands of the most abundant ^{193}IrN was obtained and the molecular constants were determined. Our observations indicate that the $a^3\Pi$ state is globally affected by other low-lying electronic states, resulting in quite different vibrational intervals in the two spin components of the excited $a^3\Pi$ state. The $a^3\Pi$ state arises from the $1\sigma^2 2\sigma^2 1\pi^4 3\sigma^1 1\delta^4\ 2\pi^1$ electronic configuration. The spectroscopic properties of the low-lying electronic states of IrN were predicted by *ab initio* calculations and our experimental assignments are supported by these calculations.

ACKNOWLEDGMENTS

We thank M. Dulick of the National Solar Observatory for assistance in obtaining the spectra. The National Solar Observatory is operated by the Association of Universities for Research in Astronomy, Inc., under contract with the National Science Foundation. The research described here was supported by funding from the NASA Laboratory Astrophysics Program. Support was also provided by the Petroleum Research Fund administered by the American Chemical Society and the Natural Sciences and Engineering Research Council of Canada. J. Liévin thanks the 'Fonds National de la Recherche Scientifique de Belgique' (Contract FRFC 2-4551.92) for financial support.

REFERENCES

1. P. W. Merrill, A. J. Deutsch, and P. C. Keenan, *Astrophys. J.* **136,** 21–34 (1962).
2. G. W. Lockwood, *Astrophys. J. Suppl. Ser.* **24,** 375–420 (1972); *Astrophys. J.* **180,** 845–855 (1973).
3. N. M. White and R. F. Wing, *Astrophys. J.* **222,** 209–219 (1978).
4. R. S. Ram, L. Wallace, and P. F. Bernath, *Astrophys. J. Suppl. Ser.* **107,** 443–449 (1996).
5. R. Yerle, *Astron. Astrophys.* **73,** 346–351 (1979).
6. B. Lindgren and G. Olofsson, *Astron. Astrophys.* **84,** 300–303 (1980).
7. D. L. Lambert and E. A. Mallia, *Mon. Not. R. Astron. Soc.* **151,** 437–447 (1971).
8. O. Engvold, H. Wöhl, and J. W. Brault, *Astron. Astrophys. Suppl. Ser.* **42,** 209–213 (1980).
9. R. S. Ram and P. F. Bernath, *J. Mol. Spectrosc.* **184,** 401–412 (1997).
10. R. S. Ram and P. F. Bernath, *J. Opt. Soc. Am. B* **11,** 225–230 (1994).
11. R. S. Ram, P. F. Bernath, W. J. Balfour, J. Cao, C. X. W. Qian, and S. J. Rixon, *J. Mol. Spectrosc.* **168,** 350–362 (1994).
12. W. J. Balfour, J. Cao, C. X. W. Qian, and S. J. Rixon, *J. Mol. Spectrosc.* **183,** 113–118 (1997).
13. R. S. Ram, J. Liévin, and P. F. Bernath, *J. Chem. Phys.* (in press).
14. A. J. Marr, M. E. Flores, and T. C. Steimle, *J. Chem. Phys.* **104,** 8183–8196 (1996).
15. R. S. Ram and P. F. Bernath, *J. Mol. Spectrosc.* **193,** 363–375 (1999).
16. E. J. Friedman-Hill and R. W. Field, *J. Chem. Phys.* **100,** 6141–6152 (1994).
17. K. Y. Jung, T. C. Steimle, D. Dai, and K. Balasubramanian, *J. Chem. Phys.* **102,** 644–652 (1995).
18. D. Dai and K. Balasubramaniam, *J. Mol. Spectrosc.* **172,** 421–429 (1995).
19. R. Scullman and B. Yttermo, *Ark. Fys.* **33,** 231–254 (1966).
20. O. Appelblad, R. F. Barrow, and R. Scullman, *Proc. Phys. Soc. London* **91,** 260–261 (1967).
21. O. Appelblad, C. Nilson, and R. Scullman, *Phys. Scr.* **7,** 65–71 (1973).
22. T. C. Steimle, K. Y. Jung, and B.-Z. Li, *J. Chem. Phys.* **102,** 5937–5941 (1995).
23. B. A. Palmer and R. Engleman, ''Atlas of the Thorium Spectrum'' Los Alamos National Laboratory, Los Alamos, 1983.
24. R. S. Ram, J. Liévin, and P. F. Bernath, *J. Chem. Phys.* **109,** 6329–6337 (1998).
25. H.-J. Werner and P. J. Knowles, *J. Chem. Phys.* **89,** 5803–5814 (1988); P. J. Knowles and H.-J. Werner, *Chem. Phys. Lett.* **145,** 514–522 (1988).
26. H.-J. Werner and P. J. Knowles, *J. Chem. Phys.* **82,** 5053–5063 (1985); P. J. Knowles and H.-J. Werner, *Chem. Phys. Lett.* **115,** 259–267 (1985).
27. S. R. Langhoff and E. R. Davidson, *Int. J. Quant. Chem.* **8,** 61–74 (1974).
28. D. Andrea, U. Häussermann, M. Dolg, H. Stoll, and H. Preuss, *Theoret. Chim. Acta* **77,** 123–141 (1990).
29. A. Bergner, M. Dolge, W. Kuechle, H. Stoll, and H. Preuss, *Mol. Phys.* **80,** 1431–1441 (1993).
30. [MOLPRO (version 96.4) is a package of *ab initio* programs written by H.-J. Werner and P. J. Knowles, with contributions of J. Almlöf, R. D. Amos, M. J. O. Deegan, S. T. Elbert, C. Hampel, W. Meyer, K. Peterson, R. Pitzer, A. J. Stone, P. R. Taylor, and R. Lindh.]
31. B. Kaving and R. Scullman, *J. Mol. Spectrosc.* **32,** 475–500 (1969).
32. H. Tan, M. Liao, and K. Balasubramaniam, *Chem. Phys. Lett.* **280,** 423–429 (1997).
33. J. M. Brown, E. A. Colbourn, J. K. G. Watson, and F. D. Wayne, *J. Mol. Spectrosc.* **74,** 425–436 (1979).
34. C. R. Brazier, R. S. Ram, and P. F. Bernath, *J. Mol. Spectrosc.* **120,** 381–402 (1986).
35. K. Jansson, R. Scullman, and B. Yttermo, *Chem. Phys. Lett.* **4,** 188–190 (1969).
36. K. Jansson and R. Scullman, *J. Mol. Spectrosc.* **36,** 248–267 (1970).